Chapter 15
Effect of Capillary Condensation on Nanoscale Friction

Rosario Capozza, Itay Barel and Michael Urbakh

Abstract While formation of capillary bridges significantly contributes to the adhesion and friction at micro- and nanoscales, many key aspects of dynamics of capillary condensation and its effect on friction forces are still not well understood. Here, by analytical model and numerical simulations, we address the origin of reduction of friction force with velocity and increase of friction with temperature, which have been experimentally observed under humid ambient conditions. We demonstrate that adding a low amplitude oscillatory component to the pulling force, when applied at the right frequency, can significantly suppress condensation of capillary bridges and thereby reduce friction. The results obtained show that frictional measurements performed in this mode can provide significant information on the mechanism of frictional aging.

15.1 Introduction

The ability to control and manipulate friction during sliding is extremely important for a large variety of applications. Development of novel efficient methods to control friction requires understanding microscopic mechanisms of frictional phenomena. One of the main difficulties in understanding and predicting frictional response is the intrinsic complexity of highly non-equilibrium processes going on in any tribological contact, which include detachment and reattachment of multiple microscopic junctions (bonds) between the surfaces in relative motion [1–8]. Even for an apparently sharp AFM tip sliding on a crystalline surface, the actual interface consists of

R. Capozza (✉)
International School for Advanced Studies (SISSA), Via Bonomea 265, I-34136 Trieste, Italy
e-mail: rosario.capozza@gmail.com

I. Barel
Department of Chemistry and Biochemistry, University of California, Santa Barbara, USA
e-mail: ibarel@chem.ucsb.edu

M. Urbakh
School of Chemistry, Tel Aviv University, Ornstein 208, Tel Aviv, Israel
e-mail: urbakh@post.tau.ac.il

E. Gnecco and E. Meyer (eds.), *Fundamentals of Friction and Wear on the Nanoscale*, NanoScience and Technology, DOI 10.1007/978-3-319-10560-4_15

an ensemble of individual junctions [9, 10]. On larger scales the multicontact picture becomes even more obvious. Friction is not simply the sum of single-junction responses, but is influenced by temporal and spatial dynamics across the entire ensemble of junctions that form the frictional interface. The way how individual junctions can be averaged to yield friction response has been the focus of intense research in the past decades [7, 8, 11–16]. These junctions may represent molecular bonds, capillary bridges, asperities between rough surfaces, and for lubricated friction they can mimic patches of solidified lubricant or its domains.

In this chapter we focus on the contribution of capillary bridges to frictional response. Important examples include the flow of granular materials [17], adhesion of insects or Geckos to surfaces [18], friction in micro- and nanoelectromechanical systems (MEMS/NEMS) [19]. Condensation of capillary bridges may be responsible for frictional ageing that is manifested as logarithmic increase of static friction with time during which two surfaces are held in stationary contact [20]. Capillary bridges play a crucial role in the operation of atomic force microscopy (AFM) under humid ambient conditions and their formation often dominates the measured forces [21–25]. Recent investigations of dependencies of frictional force on hold time, Δt, velocity, V, and temperature, T, suggested that capillary condensation is thermally activated [20–24]. It has been found that under ambient conditions the nanoscopic friction force decreases linearly with ln V at low velocities, and increases with T [21–23]. These observations disagree with predictions of thermal Prandtl-Tomlinson model of friction [26–28] and with results of experiments carried out under ultrahigh vacuum, which show a logarithmic increase of friction force with velocity and reduction of friction with temperature [29, 30]. In order to explain the observed logarithmic decrease of friction force with velocity a phenomenological model has been proposed [21] that is based on the thermally activated mechanism of nucleation of capillary bridges in a gap between asperities on the contacting surfaces. The model suggested that higher velocities correspond to shorter contact times and hence to smaller number of water bridges formed between the tip and substrate, and as a result the friction force decreases with V.

Despite importance of water bridges in frictional phenomena and the growing efforts in the field, many key aspects of dynamics of capillary condensation and its effect on friction forces are still not well understood. The present study addresses this problem through an analytical model and numerical simulations.

One unique path to controlling and ultimately manipulating the friction forces between material interfaces is through externally imposed oscillations of small amplitude and energy. Validity of this approach has been demonstrated experimentally at nano [31–33] and macroscales [34–36] and numerically with minimal models [37, 38] and molecular dynamics simulations [39, 40].

In this Chapter we demonstrate that adding a low amplitude oscillatory component to the pulling force, when applied at the right frequency, can significantly suppress the formation of capillary bridges and thereby reduce friction. The results obtained show that frictional measurements performed in this configuration can provide significant information on the kinetics of bridge formation and their stiffness.

15.2 Model

In our model and simulations we consider a rigid tip with mass M and center-of-mass coordinate X that interacts with the underlying surface through an array of contacts representing capillary bridges. The tip is pulled along the surface with a velocity V_d, through a linear spring of spring constant, K_d (see Fig. 15.1). In accordance with recent observations [21–23], we assume that nucleation of capillary bridges occurs preferentially between asperities at the tip and substrate surfaces, whose contact radius is much smaller than the AFM tip radius.

Nucleation of capillary bridges is a thermally activated process [20–24], and its rate, k_{on}, can be described by the equation

$$k_{on}^{(i)} = \omega_{on} \exp\left[-\Delta E_{on}^{i}/k_B T\right], \tag{15.1}$$

where ω_{on}, $\Delta E_{on}^{(i)}$ are the attempting frequency and the barrier height for the ith bridge. The energy barrier is proportional to the liquid volume needed to nucleate the liquid bridge, $v = a_0^2 h\,(r_i)$, where a_0^2 is a typical nucleation area and h is the gap between the surfaces at the nucleating site. The capillary bridges are characterized by a broad distribution of the barrier heights [15, 20–23, 41, 42] that leads to time-dependent increase of frictional strength, or frictional aging. Here, for simplicity we assume a uniform distribution of barrier heights above a bottom threshold, $\Delta E_{on}^{\min}$. Then a fraction of junctions with $\Delta E_{on}^{(i)} < \Delta E_{on}^{*}$ is equal to $s_E\left(\Delta E_{on}^{*} - \Delta E_{on}^{\min}\right)$, with s_E being the density of the distribution. Qualitative conclusions of this work are not sensitive to a particular choice of the distribution. It is worth pointing out that this model also describes a single capillary bridge growing with time. In this case the number of contacts represents the bridge size, while the distribution of activation energies constitutes the barrier to overcome in order to increase the size.

As long as a bridge is intact, it responds elastically to the applied force, and it can be modeled as an elastic spring with stiffness, κ [43]. Under the action of the pulling force the bridges are stretched in the lateral direction with a velocity equal to the velocity of the tip, $\dot{X}$, and therefore the tip experiences the surface force,

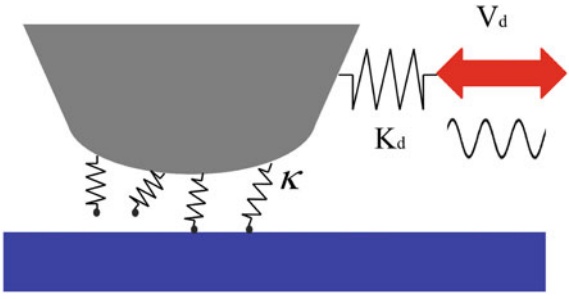

Fig. 15.1 Schematic sketch of a model geometry

$F_{cap} = -\sum_{N_s}^{i} f_i$, where $f_i = \kappa \left(l_i\,(t) - l_i^0\right), l_i(t)$ is the time-dependent bridge length, l_i^0 is the bridge length at moment of nucleation and a sum is taken over all bridges.

When the force, f_i, acting on the ith bridge exceeds the threshold value, f_c, corresponding to a maximum force that a capillary bridge can hold the bridge detaches from the tip. It should be noted that the height of the potential barrier for rupture of condensed bridges is much higher than $k_B T$ [44, 45], and because of this the effect of temperature on rupture processes is negligible.

Here for the estimation of the threshold force f_c we use the value of the maximum adhesion force (the capillary force) between the asperity and the tip that is given by the equation

$$f_c = 2\pi\gamma a_0 \left(\cos\theta_T + \cos\theta_S\right) \tag{15.2}$$

where γ is the liquid surface tension, a_0 is the average radius of asperity, and θ_T and θ_S are the contact angles at the tip and the substrate, respectively. (15.2) should be applied with caution at microscopic scales [44–46], because it relies on macroscopic concepts. It should be also noted that the maximum force that a capillary bridge can hold in the lateral direction before it breaks can be different from the maximum adhesion force in vertical direction, f_c.

In the framework of the model described above the motion of the driven tip is described by the following equation:

$$M\ddot{X} + \eta\dot{X} - F_{cap} + K_d(X - V_d t) = 0 \tag{15.3}$$

where η is a damping coefficient responsible for the dissipation of the tip kinetic energy to phonons and other degrees of freedom which are not considered explicitly here. In a wide range of parameters the results of calculations are independent of the value of η.

The instantaneous lateral spring force, which is the main observable in friction experiments, reads as $F = -K_d(X - V_d t)$, and its time average is equal to the friction force $\langle F \rangle$.

15.3 Temperature and Velocity Dependencies of Friction

The essential difference of the model described above from the previous works [14, 47, 48], where friction was described in terms of rupture and reattachment of nanoscale contacts, is a broad distribution of nucleation barriers. This leads to a long time scale dependence of number of condensed bridges on the time of contact between the tip and the substrate, and thereby to the effect of frictional aging. The average number of bridges, $N_{mf}(t)$, which are formed during the time t, can be estimated using the mean-field approach that gives [42]:

$$N(t) = N_0 \times \begin{cases} t/\tau, & t < \tau \\ ln(t/\tau) + \gamma, & t > \tau \end{cases} \tag{15.4}$$

where $N_0 = s_E k_B T$, $1/\tau = \omega_{on} \exp[-\Delta E_{on}^{\min}/k_B T]$ and $\gamma \approx 0.5572$ is the Euler-Mascheroni constant. The number of condensed bridges as a function of time shows a linear behavior at short times and logarithmic one at longer times. A logarithmic increase of number of condensed bridges with time has been already suggested in previous studies, which considered the effect of capillary condensation on friction at nano and macro scales [20, 21].

The mean field description presented above allows to describe the effect of capillary condensation on velocity and temperature dependencies of friction. When the tip is pulled with velocity V_d, the force, f_i, acting on a water bridge grows with a time-dependent rate $K_{eff} V_d / N(t)$, where $K_{eff}(t) = \frac{N(t)\kappa K_d}{N(t)\kappa + K_d}$ is the effective stiffness of the system that includes the pulling spring, K_d, and capillary bridges with total stiffness $N(t)k$. The bridge will be ruptured at the time, t_0, for which $f_i = f_c$. This yields the following equation for t_0:

$$\int_{\tau_0}^{t_0} \frac{K_{eff}}{N(t)} V_d \, dt = f_c \,, \tag{15.5}$$

where τ_0 is a time needed for nucleation of one bridge, $N(\tau_0) = 1$, and it can be estimated as $\tau_0 \approx \tau (N_0)^{-1}$. Assuming that $N(t)k \gg Kd$, (15.5) can be rewritten as $\int_{\tau_0}^{t_0} \frac{dt}{N(t)} = \frac{f_c}{K_d V_d}$. Then considering a stick-slip regime of motion, the time averaged friction force, $\langle F \rangle$, can be calculated as

$$\langle F \rangle \approx \frac{1}{2} K_d V_d (t_0 - \tau_0) \tag{15.6}$$

It should be noted that (15.5)–(15.6) have been derived under the assumption that all condensed bridges are ruptured simultaneously at the time t_0, when the force acting on one of them approaches f_c. The validity of this assumption will be tested below using stochastic simulations.

At low pulling velocities or relatively high temperatures, for which a large number of bridges are condensed during the stick phase of motion $N(t_0) \gg N_0$, the friction force can be written as

$$\langle F \rangle = f_c N_0 \Im \left(\frac{f_c N_0}{K V \tau} \right), \tag{15.7}$$

where $\Im$ is a scaling function, which depends only on one parameter, $\zeta = \frac{f_c N_0}{K V \tau}$, and increases with increasing ζ. It should be noted that both N_0 and τ are functions of temperature, and thus (15.7) provides a direct link between the temperature and velocity dependencies of friction. In particular, in the range of parameters, where $\langle F \rangle$ grows linearly with T, the average friction force decreases approximately logarithmically with velocity, $\langle F \rangle \approx const - lnV_d$. This result can be obtained substituting

(15.4) for $N(t)$ in (15.5) and neglecting the terms of the form of $ln\, ln\left[\frac{f_c N_0}{K_d V_d \tau}\right]$, which are weakly dependent on temperature and velocity.

Equation (15.7) exhibits the same characteristic friction-velocity and friction-temperature dependences as observed in the experiments [21–23]: (i) decrease of the friction force with velocity and increase with temperature, (ii) two different regimes of velocity dependence of friction for high and low pulling velocities, (iii) increase of critical velocity, V_c, for a transition between the two velocity regimes with T. In accordance with experimental observations [21–23], at low velocities $\langle F \rangle$ shows a logarithmic-like decrease with V_d, and it levels off at high velocities.

The above results have been obtained in the framework of mean field description, which is based on consideration of average number of condensed bridges, $N(t)$, and assumes that all condensed bridges are ruptured simultaneously. This is an approximation, and a more accurate approach requires a consideration of stochastic dynamics of nucleation and rupture of capillary bridges that is governed by the nucleation rates $k_{on}^{(i)}$ and coupled to the motion of tip in (15.3) [42]. Results of stochastic simulations are presented in Figs. 15.2 and 15.3, and they show velocity and temperature dependencies of friction force, and of time-averaged number of condensed bridges. One can see that the observed variations of friction force with V_d and T are entirely determined by the corresponding variations of number of condensed bridges. The proposed stochastic model enables us to describe all features of friction-velocity and friction-temperature curves, which have been observed experimentally under humid ambient conditions. The simulation parameters, f_c, ΔE_{on}^0, n_0, have been chosen to fit qualitatively the experimental data [21–23], and their values are close to those suggested by experimental studies.

The results of simulations shown in Figs. 15.2 and 15.3 are qualitatively similar to the predictions of the mean field approach [42]. However, for the same values of system parameters the friction forces obtained in the stochastic simulations are significantly higher (almost two-times) than those derived in the mean field approximation. This discrepancy results from complex dynamics of rupture and reattachment of capillary bridges, which has been observed in simulations and neglected in the approximate description. We found that part of condensed bridges is ruptured at the values of the applied force, which are considerably lower than the value needed to initiate a slip of the tip, and then they are nucleated again during the same stick interval. This effect leads to an enhancement of friction force peaks in the stick-slip series compared to those calculated in (15.5)–(15.6).

The kinetics of capillary condensation is characterized by a long-scale, logarithmic increase of number of condensed bridges with time that results in frictional ageing [20]. However, measurements of velocity and temperature dependencies of friction do not allow to distinguish this behavior from the condensation of molecular contacts characterized by a narrow distribution of nucleation barriers [42]. The only essential condition for observation of friction-velocity and friction-temperature curves similar to those in Figs. 15.2 and 15.3 is that formation of contacts (bridges) is a thermally activated process, while kinetics of rupture is temperature-independent, or only slightly influenced by T. This is different from the major assumption of

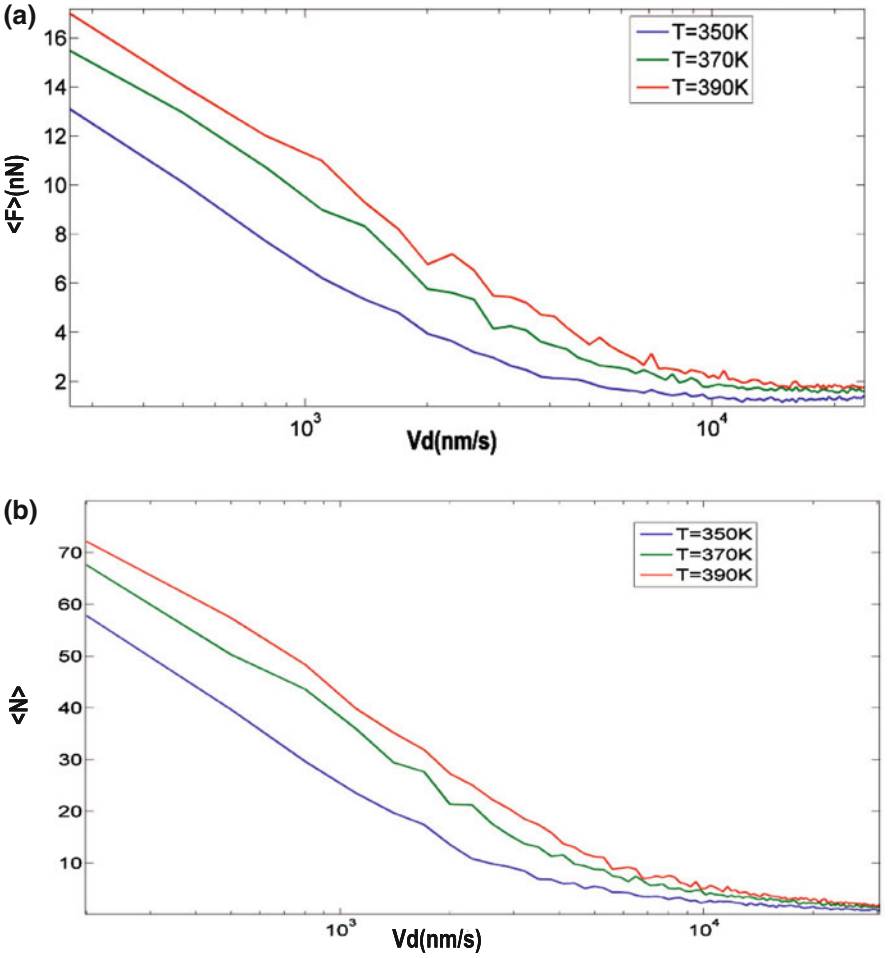

Fig. 15.2 Results of stochastic simulations for velocity dependence of the average friction force (**a**) and the average number of condensed bridges (**b**) calculated for three different temperatures. Parameter values: $M = 5 \times 10^{-11}$ kg, $\eta = 2 \times 10^{-5}$ kg/s, $f_c = 0.8$ nN, $n_0 = 2.5 \times 10^{18}$ m^{-2}, $\Delta E_{on}^0 = 4.2 \times 10^{-20}$ J, $\omega_{on}^0 = 10^7$ s^{-1}, $K = 6$ N/m, $k = 1$ N/m, $R = 30$ nm, $h_0 = 1$ nm

the standard thermally activated model of friction [26–28], according to which the rupture of nanoscale contacts (barrier crossing) is a thermally activated process. The above consideration shows that measurements of velocity and temperature dependencies of friction do not allow to draw definite conclusions on contribution of ageing processes to friction.

Nevertheless, friction measurements can provide an efficient way to study kinetics of bridge formation. This can be done using slide-hold-slide experiments [41], which are similar to slide-hold-slide tests on rocks [49, 50], where the external drive

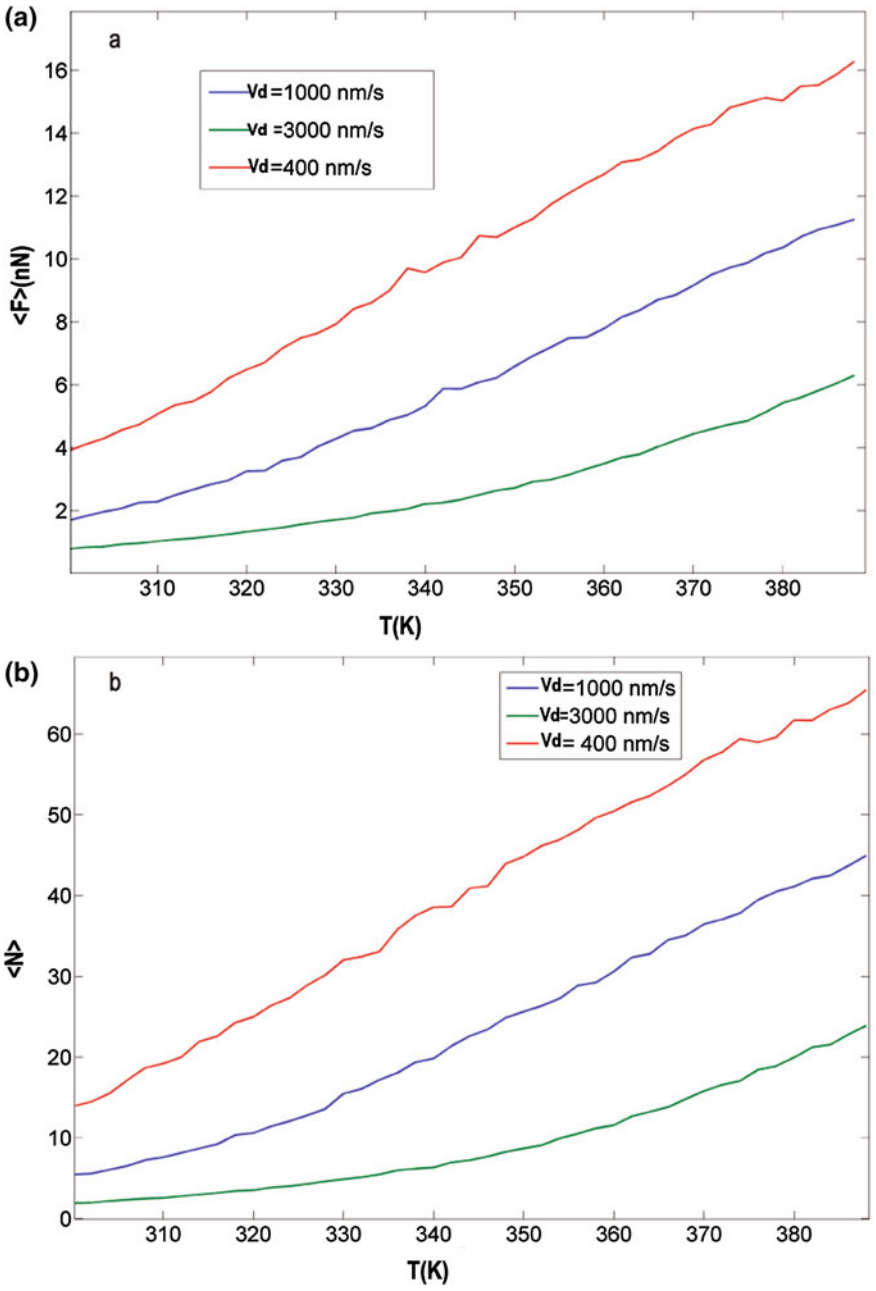

Fig. 15.3 Results of stochastic simulations for temperature dependence of the average friction force (**a**) and average number of condensed bridges (**b**) calculated for three different velocities. Parameter values as in Fig. 15.2

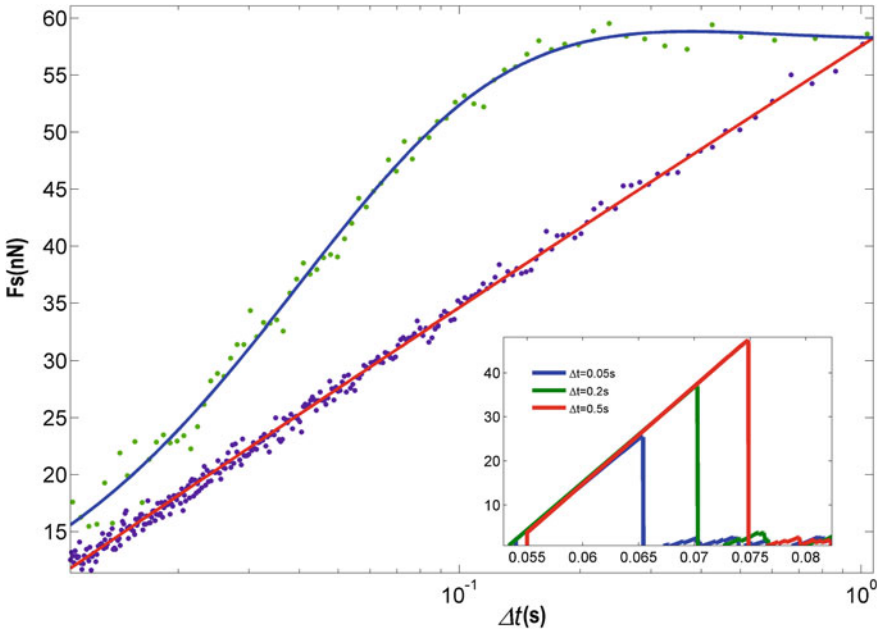

Fig. 15.4 Maximum friction force as a function of the hold time calculated for the case of capillary condensation (*green*) and for identical contacts (*purple*). The *red* and *blue* lines represent polynomial fitting curves to the calculated data. Inset shows the lateral force versus time calculated for three values of the hold time Δt. Pulling velocity, $V = 400\,\text{nm/s}$, and other parameters as in Figs. 15.4 and 15.6

is stopped for a certain hold time, Δt, and then reinitiated with the same pulling velocity, V_d. Figure 15.4 shows results of calculations of the maximum force, F_S, following specified hold periods. The presented forces have been found by averaging over hundred realizations. The maximum force is larger than the time-averaged friction force corresponding to the same velocity by an amount $\Delta F = F_s - \langle F \rangle$, called friction drop. For capillary condensation of bridges F_S, grows linearly with the logarithm of the hold time showing a strong effect of ageing on nanoscopic friction that results from a broad distribution of activation energy barriers for capillary condensation. In the case of identical contacts significant deviations from the logarithmic dependence are observed already for $\Delta t \geq 3\tau$. Thus, our simulations demonstrate that slide-hold-slide experiments can provide important information on kinetics of bridge formation and mechanism of frictional ageing.

Figure 15.4 shows that in the case of capillary condensation the calculated relative friction drop, $\Delta F / \langle F_s \rangle$ increases about ten times as the hold time increased by two orders of magnitude. This result is consistent with recent nanoscopic friction measurements [41], which found ten times increase of relative friction drop, when the hold time increased by two orders of magnitude. The magnitude of the ageing effect for the nanoscale single asperity contacts that has been found in experiments [41] and

in our simulations is much larger than for macroscopic multi-asperity friction experiments [49–51]. However, it should be noted that in the cited experiments the large ageing effect has been observed also for low humidities showing that the capillary condensation is not the only mechanism for frictional ageing. Further experimental and theoretical studies are needed to address the mechanisms that account for this.

15.4 Effect of Inplane Oscillations

In order to study the effect of inplane oscillatory modulation on friction, we add a low amplitude oscillatory component to the ramped forces. Then the displacement of the stage reads as $X_d = V_d t + A \cos(2\pi \upsilon t)$ where V_d is a constant velocity, υ and A are the frequency and amplitude of oscillations. When the tip is pulled with constant velocity, time series of the spring force exhibit stick-slip behavior corresponding to collective rupture and reattachment of capillary bridges (see Fig. 15.5a). Once small harmonic perturbations are introduced to the ramped loading, this picture changes significantly. Figure 15.5b shows that for frequencies of oscillations above a threshold one, υ_{th}, the force traces represent a set of alternating segments of stick-slip oscillation and low friction sliding, which are marked as t_{s-s} and t_{lag}, respectively [52]. For high frequencies (green curve in Fig. 15.6a) the stick-slip oscillations are completely suppressed and the spring force remains low over the entire time of

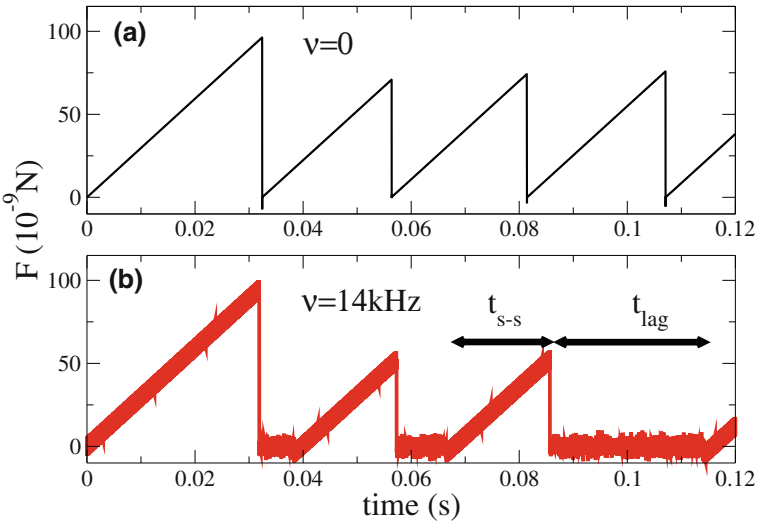

Fig. 15.5 **a** Typical stick-slip profile obtained when the tip is pulled with constant velocity. **b** Force trace corresponding to lateral modulations with the amplitude A = 1 nm and υ = 14 kHz. The trace shows alternating segments of stick-slip and low friction motion with durations t_{s-s} and t_{lag}, respectively

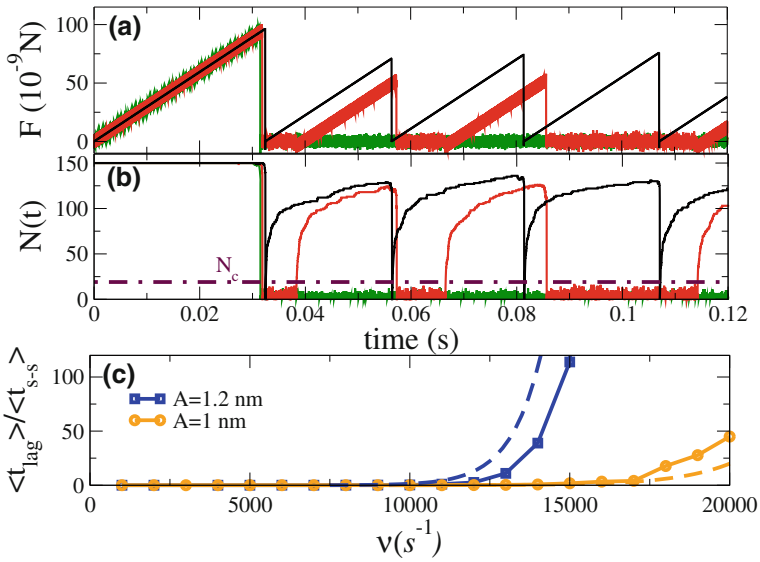

Fig. 15.6 **a** Force traces and **b** time-dependent number of condensed bridges, N(t), calculated in the absence of oscillations (*black curves*) and including the oscillatory component of the force with A = 1nm and υ = 14 kHz (*red curves*) and υ = 19.6 kHz (*green curves*). *Dashed-dotted line* in the panel (**b**) indicates the maximal number of bridges, N_c, which can be ruptured by the oscillatory modulations with the amplitude A = 1 nm estimated using (15.8). **c** Ratio $\langle t_{lag} \rangle / \langle t_{s-s} \rangle$ as a function of υ for two amplitudes of oscillations which are indicated in the figure. *Solid* and *dashed curves* present results of simulations and analytical theory, respectively

simulations shown in Fig. 15.6a. In order to elucidate the mechanism of reduction of friction we show in Fig. 15.6b the effect of oscillations on the time-dependent number of condensed bridges, *N(t)*. While in the absence of oscillations *N(t)* starts to grow monotonically directly after the slip event, application of small-amplitude oscillations suppresses the formation of capillary bridges during finite time-intervals, t_{lag}. This effect results in a low friction regime of motion corresponding to uncorrelated rupture of small clusters of bridges. Because of stochastic nature of bridge formation, the regime of low friction motion persists only for a finite time, t_{lag} until the number of bridges formed during a half-period of oscillations becomes larger than a critical value N_c that cannot be ruptured by the oscillatory component of force, as shown by dashed-dotted line in Fig. 15.6b. Then, oscillatory modulations become inefficient, and the number of bridges grows until the ramped component of the loading force causes the collective rupture of bridges similar to what happens in the absence of modulations. The value of loading force corresponding to the collective rupture in the presence of modulation is only slightly below the maximal force for constant velocity pulling (see Fig. 15.6a) and it depends weakly on υ. However, the length of the time-intervals of low friction, t_{lag}, increases rapidly with υ and as a result the average friction force decreases.

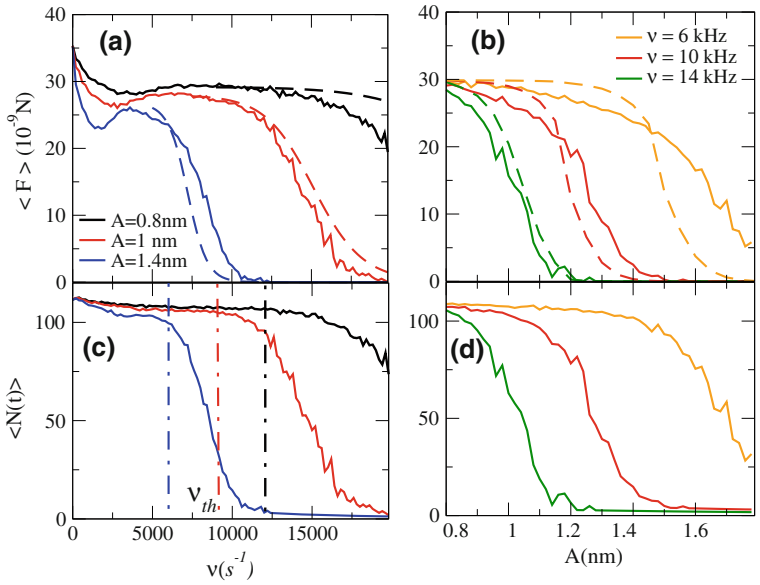

Fig. 15.7 Average friction force, $\langle F \rangle$, as a function of frequency (**a**) and amplitude (**b**) of oscillations, and the corresponding variations of average number of condensed bridges, $\langle N(t) \rangle$, reported in panels (**c**) and (**d**). *Solid and dashed curves* in (**a**) and (**b**) show results of simulations and analytical calculations according to (15.12), respectively. *Vertical dashed-dotted lines* in (**c**) present analytical estimations of the threshold frequency, υ_{th}, corresponding to different values of the amplitude A

Figure 15.6c shows the ratio $\langle t_{lag} \rangle / \langle t_{s-s} \rangle$ as a function of υ for two amplitudes of oscillation, where $\langle t_{lag} \rangle$ and $\langle t_{s-s} \rangle$ are the mean values of t_{lag} and t_{s-s} which have been calculated by averaging over a large number of realizations. Inplane oscillations induce nonzero time-intervals of low friction, t_{lag}, only for frequencies exceeding a threshold value, υ_{th}, which decreases with the amplitude of oscillations. Above the threshold frequency, $\langle t_{lag} \rangle / \langle t_{s-s} \rangle$ increases sharply with υ and the average friction force is reduced. It should be noted that over the entire range of data presented, the amplitude of the applied force oscillations was lower than the tenth of the force needed to initiate a slip of the tip in the case of constant velocity pulling. Thus, despite strong effects on stick-slip dynamics the perturbations are decidedly small.

Figure 15.7 presents the average friction force, $\langle F \rangle$, and the average number of condensed capillary bridges, $\langle N(t) \rangle$, as functions of frequency and amplitude of oscillations. One can see that for a given amplitude, $N(t)$ decreases steeply above a threshold frequency, υ_{th} (A), and the friction force follows this behavior. Figure 15.7b demonstrate a similar reduction of $\langle N(t) \rangle$ and $\langle F \rangle$ with increase of the amplitude of oscillations for a given frequency. Thus, application of small amplitude oscillations with frequencies of few kHz allows to reduce the friction force by more than one order of magnitude.

The mechanism of reduction of friction discussed here differs significantly from those suggested in previous works [32, 40] on the effects of oscillatory modulations on friction. It can operate only in tribological contacts exhibiting aging where times for bridge formation are widely distributed or there is a long time-scale strengthening of bridges. In these systems a frequency of force modulations can be chosen in a way that only a small number of bridges is formed during the half-period of oscillations, and these "fresh" bridges can be ruptured by the oscillatory component of the loading force. Thus, small inplane oscillations are able to prevent the formation of multiple bridges and reduce friction. In order to achieve similar reduction of friction in contacts characterized by a narrow distribution of times for bridge formation (in the absence of aging) much higher amplitudes or/and frequencies of modulation are required.

The main features of numerical results presented above can be reproduced by an analytical model based on a mean field description of ensemble of bridges that has been discussed above. When the tip is pulled with the velocity $\dot{X}_d$, the force, f_i, acting on a bridge grows with a time-dependent rate $K_{eff}\dot{X}_d/N(t)$, where $K_{eff}(t) = \frac{N(t)\kappa K_d}{N(t)\kappa+K_d}$ is the effective stiffness of the system. Assuming that all bridges are ruptured simultaneously at time t, when the force acting on one of them approaches f_c, the condition for a collective rupture is given by (15.5). This equation allows to estimate the key parameters which define the effect of oscillations on friction, such as: the maximal number of capillary bridges, N_c, which can be ruptured by the oscillatory modulations, and the threshold frequency, υ_{th}, above which the force oscillations produce low friction segments of motion. Considering that rupture occurs at a time corresponding to the maximum of the oscillatory force, $t = T_\upsilon = 1/(2\,\upsilon)$, and using (15.4) for *N(t)* we get the following approximate equation for $N_c = N(T_\upsilon)$:

$$N_c \frac{\kappa}{K_d}\left(1 - \frac{f_c}{4AK_d}N_c\right) = ln\left(1 + \frac{\kappa}{K_d}N_c\right) \tag{15.8}$$

Then, for a linear regime of growth of *N(t)* in (15.4) the threshold frequency can be estimated as $\upsilon_{th} \simeq \frac{N_0}{2\tau N_c}$. Estimations of N_c and $\upsilon_{th}(A)$ reported in Figs. 15.6b and 15.7c, respectively, show a good agreement with the results of simulations.

In order to describe the effect of oscillations on friction we have to consider a stochastic nature of bridge formation. The number of bridges formed during the half-period of oscillations fluctuates around an average value $N(T_\upsilon)$ given by (15.4). While *N(t)* is below the critical value, N_c, the spring force, *F(t)*, remains low but if during one of the oscillations $N(T_\upsilon)$ exceeds N_c the force oscillations become inefficient and *F(t)* grows. The probability, *P(m,t)*, of formation of m bridges in time t is given by a sum of probabilities of formation of all possible clusters of bridges of size m. In the case of identical bridges, *P(m,t)* can be easily calculated taking into account that there are $\frac{N_s!}{(N_s-m)!m!}$ clusters of size m, where N_s is a total number of available bridges. However, in systems exhibiting aging, different bridges have different barrier heights ΔE^i_{on}, and correspondingly different probabilities of formation which can be calculated as, $P_i(t) = 1 - exp\left(-k^i_{on}\,t\right)$, where k^i_{on} is the rate of formation of i-th bridge given by (15.1). Then, the probability $P(m,t)$ can

be found using the recursive equation [53]

$$P(m,t) = \begin{cases} \prod_{i=1}^{N_s} (1 - P_i(t)), & m = 0 \\ \frac{1}{m} \sum_{i=1}^{N_s} (-1)^{i-1} P(m-i,t) Q_i(t), & m > 0 \end{cases} \tag{15.9}$$

where $Q_i(t) = \sum_{j=1}^{N_s} \left(\frac{P_j(t)}{1-P_j(t)}\right)^i$. Then the average length of the time-interval, $\langle t_{lag} \rangle$, during which the number of condensed bridges is below N_c, and the spring force remains low, can be calculated as

$$\langle t_{lag} \rangle = \frac{T_\upsilon}{\tilde{P}(N_c, T_\upsilon)} \tag{15.10}$$

where $\tilde{P}(N_c, T_\upsilon) = \sum_{i=1}^{+\infty} P(i, T_\upsilon)$ is a probability that no less than N_c bridges are formed during the time T_υ.

As the frequency increases, the probability $\tilde{P}(N_c, T_\upsilon)$ decreases rapidly and $\langle t_{lag} \rangle$ increases. Dashed curves in Fig. 15.6c present results of analytical calculations of $\langle t_{lag} \rangle$ in (15.10), which agree qualitatively with the results of numerical simulations discussed above.

Considering that in the presence of oscillatory modulations the force series represent the set of alternating segments of stick-slip oscillations and low friction sliding (see Figs. 15.5 and 15.6), the average friction force can be estimated as

$$\langle F \rangle = \frac{\langle F_{s-s} \rangle \langle t_{s-s} \rangle}{\langle t_{s-s} \rangle + \langle t_{lag} \rangle} \tag{15.11}$$

where $\langle t_{s-s} \rangle / \left(\langle t_{s-s} \rangle + \langle t_{lag} \rangle \right)$ is a fraction of time corresponding to the stick-slip state of motion, $\langle F_{s-s} \rangle$ is the average force experienced by the tip in that state, and the contribution of the low friction sliding was neglected. Approximating by $\langle F_{s-s} \rangle \cong \frac{K_d V_d \langle t_{s-s} \rangle}{2}$, we get the following equation for the average friction force

$$\langle F \rangle = \frac{2 \langle F_{s-s} \rangle^2}{2 \langle F_{s-s} \rangle + K_d V_d \langle t_{lag} \rangle} \tag{15.12}$$

With increase of A or/and υ the length of low friction segments $\langle t_{lag} \rangle$ grows and the friction force decreases rapidly. Dashed curves in Fig. 15.7a, b show $\langle F \rangle$ as functions of frequency and amplitude of modulations which have been calculated according to the (15.12). The analytical results are in qualitative agreement with numerical simulations. It should be noted that the mean field description given by

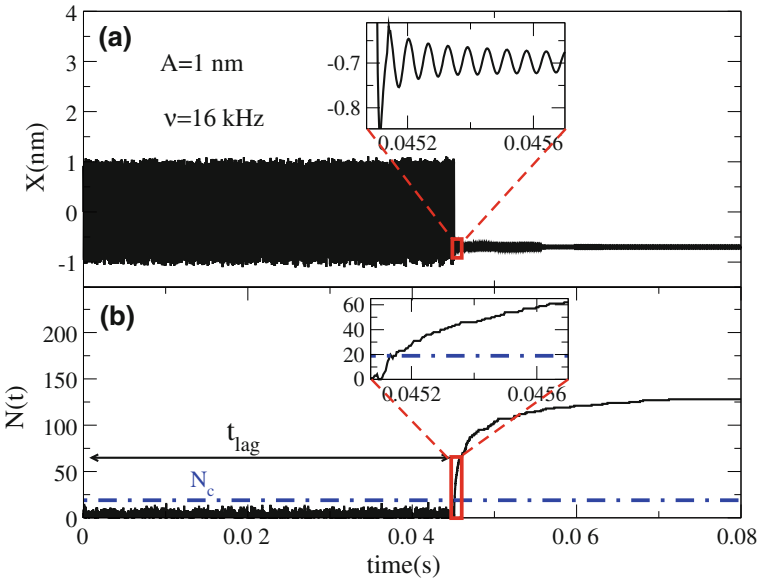

Fig. 15.8 **a** Displacement of the tip, X(t), as a function of time in response to harmonic driving. The tip is brought in contact with a substrate at t = 0. **b** Dynamics of bridge formation, N(t). *Dashed dotted line* in the panel (**b**) indicates the maximal number of junctions, N_c, which can be ruptured by the oscillatory modulations with the amplitude A = 1.0 nm. The insets zoom in the region corresponding to the transition from the low to high friction state

(15.5), (15.8)–(15.12) assumes that bridges are ruptured simultaneously under the action of the pulling force and $\langle F_{s-s} \rangle$ is independent on A. These assumptions are inaccurate for high amplitudes and frequencies of oscillation, and in this range of parameters the analytical results deviate essentially from the numerical ones (see Fig. 15.7a, b).

Our simulations suggest that applying small-amplitude inplane oscillations to the stage of AFM one can give important information on the kinetics of frictional aging and the stiffness of bridges. In order to do this we propose to bring the oscillating tip in contact with the surface and to follow the time variation of the amplitude of the tip oscillations, A_{tip}. Figure 15.8 shows the tip motion and the kinetics of capillary bridges formation for the tip that is driven at the velocity $V_d = -2\pi\nu A \sin(2\pi\nu t)$ and brought in the contact at t = 0. The tip exhibits high amplitude oscillations for the time interval $t < t_{lag}$ during which the formation of bridges is suppressed by oscillations. In this regime the amplitude of tip oscillations, A_{tip}, is only slightly below the driving amplitude A = 1 nm, as shown in Fig. 15.8a. When the number of bridges formed during a half-period of oscillations exceeds the critical one, N_c, (inset in Fig. 15.8b) the cluster of condensed bridges starts to grow and the amplitude, A_{tip}, is greatly reduced as shown in Fig. 15.8a. Considering the balance of forces acting on the tip, $A_{tip}(t)\, N(t)\kappa = \left(A - A_{tip}(t)\right) K_d$, the time variation of the amplitude of tip

oscillations can be related to the time-dependent stiffness of the cluster of condensed bridges,

$$N(t)\kappa = K_d\left(\frac{A}{A_{tip}(t)} - 1\right) \tag{15.13}$$

Thus the proposed measurements can provide direct information on the kinetics of frictional aging and the stiffness of bridges. Additional information on the distribution of heights of barriers for bridge formation can be obtained comparing the measured values of t_{tag} with the results of calculations according (15.10). This comparison allows to estimate the main parameters of the distribution of the barrier heights, such as the minimal barrier height, $\Delta E_{on}^{\min}$, and the density, S_E.

15.4.1 Summary

Capillary bridges play a crucial role in the operation of atomic force microscopy under humid ambient conditions and their formation often dominates the measured forces. It has been found that under ambient conditions the nanoscopic friction force decreases with pulling velocities and increases with temperature [21–23]. These observations differ significantly from the results of friction experiments carried out under ultrahigh vacuum, and disagree with predictions of thermal Prandtl-Tomlinson model of friction. Here, by analytical model and numerical simulations, we demonstrate that the observed friction phenomena are caused by the fact that formation of capillary bridges is a thermally activated process, while kinetics of their rupture is temperature-independent, or only slightly influenced by T. Our calculations show that measurements of velocity and temperature dependencies of friction force do not allow to draw definite conclusions on contribution of ageing processes to friction. However, we found that this information can be provided by slide-hold-slide measurements.

We demonstrated that adding a low amplitude oscillatory component to the pulling force, when applied at the right frequency, can significantly suppress formation of capillary bridges and thereby reduce friction. Our simulations suggest that applying small-amplitude inplane oscillations to the stage of AFM one can get direct information on the kinetics of frictional aging and the stiffness of capillary bridges.

Acknowledgments We grateful to R. W. Carpick, A.E. Filippov, C. Greiner, P.-E. Mazeran and O. Noel for helpful discussions. R.C. acknowledges support from the Swiss National Science Foundation SINERGIA Project CRSII2 136287\1. The work was supported by DIP (German-Israeli Project Cooperation Program) and the Israel Science Foundation (1109/09).

References

1. M. Urbakh, J. Klafter, D. Gourdon, J. Israelachvili, The nonlinear nature of friction. Nature **430**, 525–528 (2004)
2. V. Bormuth, V. Varga, J. Howard, E. Schaffer, Protein Friction Limits Diffusive and Directed Movements of Kinesin Motors on Microtubules. Science **325**, 870–873 (2009)
3. C.H. Scholz, Earthquakes and friction laws. Nature **391**, 37–42 (1998)
4. R. Budakian, S.J. Putterman, Correlation between charge transfer and stick-slip friction at a metalinsulator interface. Phys. Rev. Lett. **85**, 1000 (2000)
5. E. Gerde, M. Marder, Friction and fracture. Nature (London) **413**, 285 (2001)
6. A.E. Filippov, J. Klafter, M. Urbakh, Friction through dynamical formation and rupture of molecular bonds. Phys. Rev. Lett. **92**, 135503 (2004)
7. S.M. Rubinstein, G. Cohen, J. Fineberg, Detachment fronts and the onset of dynamic friction. Nature **430**, 1005 (2004)
8. A. Vanossi, N. Manini, M. Urbakh, S. Zapperi, E. Tosatti, Colloquium: modeling friction: from nanoscale to mesoscale. Rev. Mod. Phys. **85**, 529 (2013)
9. Y. Mo, K.T. Turner, I. Szlufarska, Friction laws at the nanoscale. Nature **457**, 1116–1119 (2009)
10. B. Gotsmann, M.A. Lantz, Quantized thermal transport across contacts of rough surfaces. Nature Mater. **12**, 59–65 (2012)
11. B.N.J. Persson, *Sliding Friction: Physical Principles and Applications* (Springer, Berlin, 1998)
12. O.M. Braun, M. Peyrard, Modeling friction on a mesoscale: master equation for the earthquakelike model. Phys. Rev. Lett. **100**, 125501 (2008)
13. O.M. Braun, I. Barel, M. Urbakh, Dynamics of transition from static to kinetic friction. Phys. Rev. Lett. **103**, 194301 (2009)
14. I. Barel, M. Urbakh, L. Jansen, A. Schirmeisen, Multibond dynamics of nanoscale friction: the role of temperature. Phys. Rev. Lett. **104**, 066104 (2010)
15. Y. Liu, I. Szlufarska, Chemical origins of frictional aging. Phys. Rev. Lett. **109**, 186102 (2012)
16. R. Capozza, M. Urbakh, Static friction and the dynamics of interfacial rupture. Phys. Rev. B **86**, 085430 (2012)
17. T.C. Halsey, A.J. Levine, How sandcastles fall. Phys. Rev. Lett. **80**, 3141 (1998)
18. S.N. Gorb, *Attachment Devices of Insect Cuticle* (Kluwer Academic Publishers, Dordrecht, 2001)
19. B. Bhushan, *Handbook of Nanotribology* (Springer, New York, 2007)
20. L. Bocquet, E. Charlaix, S. Ciliberto, J. Crassous, Moisture-induced ageing in Granular media and the kinetics of capillary condensation. Nature (London) **396**, 735 (1998)
21. E. Riedo, F. Le'vy, H. Brune, Kinetics of capillary condensation in nanoscopic sliding friction. Phys. Rev. Lett. **88**, 185505 (2002)
22. R. Szoszkiewicz, E. Riedo, Nucleation time of nanoscalewater bridges. Phys. Rev. Lett. **95**, 135502 (2005)
23. C. Greiner, J.R. Felts, Z. Dai, W.P. King, R.W. Carpick, Local nanoscale heating modulates single-asperity friction. Nano Lett. **10**, 4640 (2010)
24. O. Noel, P.-E. Mazeran, H. Nasrallah, Sliding velocity dependence of adhesion in a nanometer-sized contact. Phys. Rev. Lett. **108**, 015503 (2012)
25. L. Zitzler, S. Herminghaus, F. Mugele, Capillary forces in tapping mode atomic force microscopy. Phys. Rev. B **66**, 155436 (2002)
26. Y. Sang, M. Dube, M. Grant, Thermal effects on atomic friction. Phys. Rev. Lett. **87**, 17430 (2001)
27. O.K. Dudko, A.E. Filippov, J. Klafter, M. Urbakh, Dynamic force spectroscopy: a Fokker−Planck approach. Chem. Phys. Lett. **352**, 499 (2002)
28. I. Szlufarska, M. Chandross, R.W. Carpick, Recent advances in single-asperity nanotribology. J. Phys. D **41**, 123001 (2008)
29. E. Gnecco, R. Bennewitz, T. Gyalog, C. Loppacher, M. Bammerlin, E. Meyer, H.J. Guntherodt, Velocity dependence of atomic friction. Phys. Rev. Lett. **84**, 1172–1175 (2000)

30. L. Jansen, H. Holscher, H. Fuchs, A. Schirmeisen, Temperature dependence of atomic-scale stick-slip friction. Phys. Rev. Lett. **104**, 256101 (2010)
31. M. Heuberger, C. Drummond, J.N. Israelachvili, Coupling of normal and transverse motion during frictional sliding. J. Phys. Chem. B **102**, 5038 (1998)
32. A. Socoliuc et al., Atomic-scale control of friction by actuation of nanometer- sized contacts. Science **313**, 207 (2006)
33. S. Jeon, T. Thundat, Y. Braiman, Effect of normal vibration on friction in the atomic force microscopy experiment. Appl. Phys. Lett. **88**, 214102 (2006)
34. A. Cochard, L. Bureau, T. Baumberger, Stabilization of frictional sliding by normal load modulation: a bifurcation analysis. Trans. ASME **70**, 220 (2003)
35. V.L. Popov, J. Starcevic, A.E. Filippov, Influence of ultrasonic in-plane oscillations on static and sliding friction and intrinsic length scale of dry fiction. Tribol. Lett. **39**, 25 (2010)
36. R. Capozza, S.M. Rubinstein, I. Barel, M. Urbakh, J. Fineberg, Stabilizing stick-slip friction. Phys. Rev. Lett. **107**, 024301 (2011)
37. M.G. Rozman, M. Urbakh, J. Klafter, Controlling chaotic frictional forces. Phys. Rev. E **57**, 7340 (1998)
38. Z. Tshiprut, A.E. Filippov, M. Urbakh, Tuning diffusion and friction in microscopic contacts by mechanical excitations. Phys. Rev. Lett. **95**, 016101 (2005)
39. J.P. Gao, W.D. Luedtke, U. Landman, Friction control in thin-film lubrication. J. Phys. Chem. B **102**, 5033–5037 (1998)
40. R. Capozza, A. Vanossi, A. Vezzani, S. Zapperi, Suppression of friction by mechanical vibrations. Phys. Rev. Lett. **103**, 085502 (2009)
41. Q. Li, T.E. Tullis, D. Golldsby, R.W. Carpick, On the origins of rate and state friction: frictional ageing from interfacial bonding. Nature (London) **480**, 233 (2011)
42. I. Barel, A.E. Filippov, M. Urbakh, Formation and rupture of capillary bridges in atomic scale friction. J. Chem. Phys. **137**, 164706 (2012)
43. H. Choe, M.-H. Hong, Y. Seo, K. Lee, G. Kim, Y. Cho, J. Ihm, W. Jhe, Formation, manipulation, and elasticity measurement of a nanometric column of water molecules. Phys. Rev. Lett. **95**, 187801 (2005)
44. M. He, A.S. Blum, D.E. Aston, C. Buenviaje, R.M. Overney, R. Luginbuhl, Critical phenomena of water bridges in nanoasperity contacts. J. Chem. Phys. **114**, 1355 (2001)
45. J. Crassous, M. Ciccotti, E. Charlaix, Capillary, force between wetted nanometric contacts and its application to atomic force microscopy. Langmuir **27**, 3468 (2011)
46. H.-J. Butt, Capillary forces: influence of roughness and heterogeneity. Langmuir **24**, 4715 (2008)
47. I. Barel, M. Urbakh, L. Jansen, A. Schirmeisen, Temperature dependence of friction at the nanoscale: when the unexpected turns normal. Trib. Lett. **39**, 311 (2010)
48. I. Barel, M. Urbakh, L. Jansen, A. Schirmeisen, Unexpected temperature and velocity dependencies of atomic-scale stick-slip friction. Phys. Rev. B **84**, 115417 (2011)
49. J.H. Dieterich, Modeling of rock friction: 1. experimental results and constitutive equations. J. Geophys. Res. **84**, 2161 (1979)
50. V.L. Popov, *Contact Mechanics and Friction: Physical Principles and Applications* (Springer, Berlin, 2010)
51. K.M. Frye, C. Marone, Effect of humidity on granular friction at room temperature. J. Geophys. **107**, 2309 (2002)
52. R. Capozza, I. Barel, M. Urbakh, Probing and tuning frictional aging at the Nanoscale. Sci. Rep. **3**, 1896 (2013)
53. X.H. Chen, A.P. Dempster, J.S. Liu, Weighted finite population sampling to maximize entropy. Biometrika **81**(3), 457 (1994)